J Digit Imaging
https://doi.org/10.1007/s10278-017-0033-z

Application of Super-Resolution Convolutional Neural Network for Enhancing Image Resolution in Chest CT

Kensuke Umehara[1] · **Junko Ota**[1] · **Takayuki Ishida**[1]

Abstract In this study, the super-resolution convolutional neural network (SRCNN) scheme, which is the emerging deep-learning-based super-resolution method for enhancing image resolution in chest CT images, was applied and evaluated using the post-processing approach. For evaluation, 89 chest CT cases were sampled from The Cancer Imaging Archive. The 89 CT cases were divided randomly into 45 training cases and 44 external test cases. The SRCNN was trained using the training dataset. With the trained SRCNN, a high-resolution image was reconstructed from a low-resolution image, which was down-sampled from an original test image. For quantitative evaluation, two image quality metrics were measured and compared to those of the conventional linear interpolation methods. The image restoration quality of the SRCNN scheme was significantly higher than that of the linear interpolation methods ($p < 0.001$ or $p < 0.05$). The high-resolution image reconstructed by the SRCNN scheme was highly restored and comparable to the original reference image, in particular, for a ×2 magnification. These results indicate that the SRCNN scheme significantly outperforms the linear interpolation methods for enhancing image resolution in chest CT images. The results also suggest that SRCNN may become a potential solution for generating high-resolution CT images from standard CT images.

✉ Kensuke Umehara
kensuke.umehara@ieee.org

Junko Ota
junko.76.ota@gmail.com

Takayuki Ishida
tishida@sahs.med.osaka-u.ac.jp

[1] Department of Medical Physics and Engineering, Graduate School of Medicine, Osaka University, 1-7 Yamadaoka, Suita 565-0871, Japan

Keywords Super resolution · Deep learning · Artificial intelligence · Super-resolution convolutional neural network · High-resolution medical imaging · Computed tomography

Introduction

High-resolution imaging has recently attracted much attention in the field of medical imaging, and it is expected to lead to more accurate diagnosis [1]. In computed tomography (CT), high-resolution CT (HRCT) is an essential diagnostic tool for identifying some pulmonary diseases such as pulmonary tuberculosis [2], idiopathic pulmonary fibrosis [3], and interstitial pneumonia [4]. HRCT outperforms conventional chest CT when identifying and distinguishing various entities of interstitial lung disease [5, 6]. However, the acquisition of volumetric HRCT images requires state-of-the-art multidetector CT scanners (e.g., at least 16 detector rows). The scanning time of HRCT images with conventional CT scanners (e.g., 4 detector rows) is considerably long, with most patients unable to hold their breath long enough for complete lung scan [7]. If the acquisition of high-resolution CT images from standard CT images by using post-processing is made possible, it could improve the overall visualization of small anatomical structures and will lead to more accurate diagnosis.

The simplest approach to generating a high-resolution image by post-processing is through linear interpolation methods such as the nearest neighbor, bilinear, and bicubic interpolations. These methods are widely used for improving the resolution of a low-resolution image. However, conventional linear interpolation methods often produce over-smoothed images with artifacts such as aliasing, blur, and halo around the edges [8].

The super-resolution method is the process of estimating a high-resolution image from a low-resolution input image, which can reduce artifacts resulting from the conventional linear

Published online: 18 October 2017

interpolation methods. Recent super-resolution methods are example-based methods that learn the relationship between low-resolution and high-resolution image pairs. In computer vision, various example-based super-resolution methods have been proposed [9–11]. It has been shown that the use of the sparse-coding super-resolution method [10], which is an example-based super-resolution method, yielded higher image quality over that of the conventional linear interpolation methods in chest CT images [12]. However, for real-time clinical applications in medical imaging, the computation time of the conventional example-based super-resolution methods still remains a challenge.

Deep learning, also known as deep convolutional neural network (DCNN), has revolutionized the application of a large number of computer vison problems, including image enhancement, such as denoising [13] and deblurring [14]. In super-resolution, the super-resolution convolutional neural network (SRCNN) [15, 16] scheme, which is a deep-learning-based super-resolution method, has recently been proposed in the field of computer vision. The SRCNN scheme can directly learn an end-to-end mapping between the low-resolution image and the high-resolution image. Recent studies have shown that the use of the SRCNN scheme for non-medical imaging achieved superior performance over the previous super-resolution methods in terms of image quality and processing speed [15, 16]. In medical imaging, it has been shown that the application of the SRCNN scheme to chest radiographs could significantly improve image quality of high-resolution images in comparison with the use of the conventional linear interpolation methods [17, 18]. However, few studies have investigated whether the application of the SRCNN scheme contributes to the improvement of the image quality of high-resolution images in CT images.

In this paper, the SRCNN scheme was applied and evaluated for enhancing image resolution in chest CT images by post-processing. The performance of the SRCNN scheme for the improvement of the image quality of high-resolution images was evaluated using clinical CT cases. In addition, the training schemes for improving the image quality of the reconstructed high-resolution images were explored. Two types of training images—non-medical images and chest CT images—were used as the training dataset.

Materials and Methods

Materials

In all, 89 chest CT images of patients diagnosed with non-small cell lung cancer, who were surgically treated [19, 20], were obtained from The Cancer Imaging Archive (TCIA) [21]. The TCIA is a publicly available open-access database provided by the National Cancer Institute. The 89 chest CT cases were divided randomly into a training dataset and an external test dataset. The training dataset contained 45 chest CT cases and the test dataset contained 44 chest CT cases.

Super-Resolution Convolutional Neural Network

Figure 1 shows an overview of the SRCNN [15, 16] that was used in this study. The SRCNN scheme requires bicubic interpolation-based upscaling, which is the only pre-processing step involved. The SRCNN is a feed-forward network that can be divided into three steps—patch extraction and representation, non-linear mapping, and reconstruction.

The patch-extraction-and-representation part extracts patches from the bicubic interpolated low-resolution input image. The first layer is expressed as follows:

$$F_1(Y) = \max(0, W_1 * Y + B_1), \quad (1)$$

where F, $\mathbf{Y}$, W_1, and B_1 represent the mapping function, the bicubic interpolated low-resolution image, the filters, and the biases, respectively. W_1, which has a size of $c \times f_1 \times f_1$, corresponds to n_1 filters, where c is the number of channels in the input image, n_1 is the number of filter sizes, and f_1 is the spatial size of a filter. The output is composed of n_1 feature maps, and

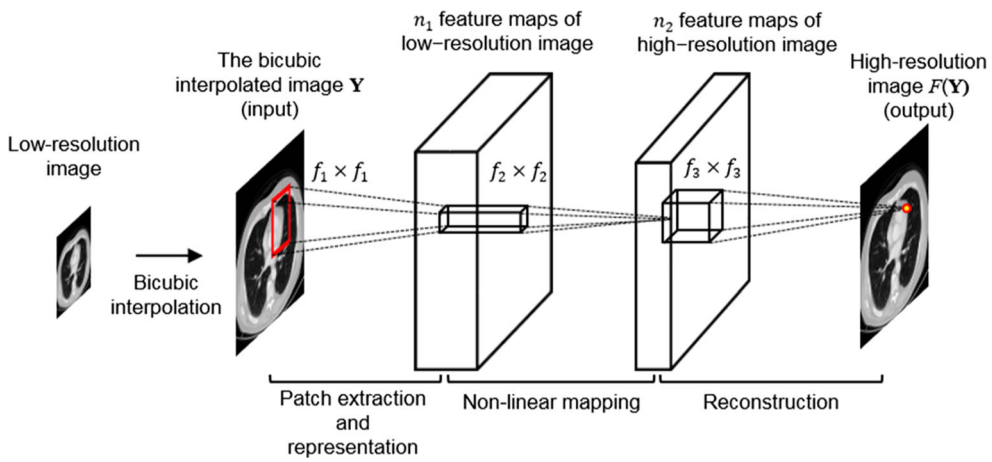

Fig. 1 Architecture of the super-resolution convolutional neural network (SRCNN) scheme used in this study

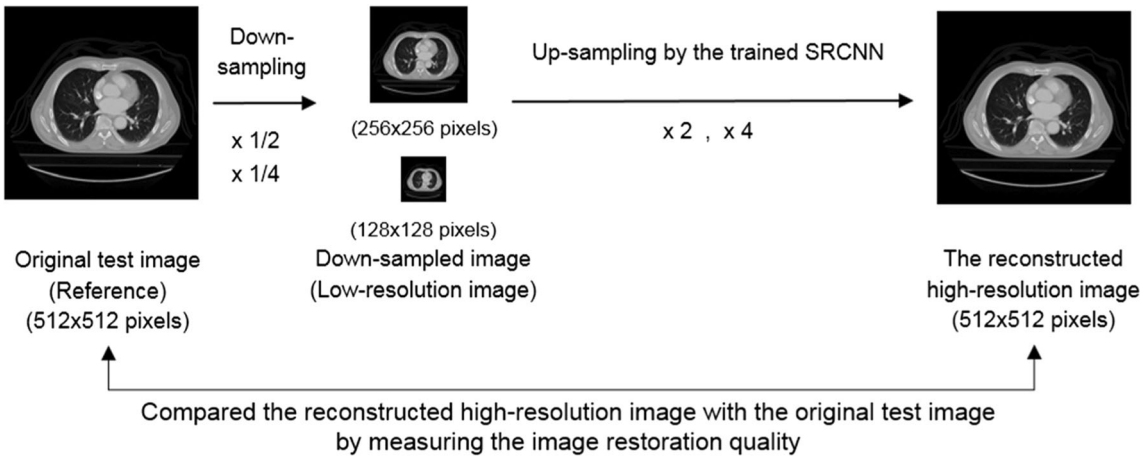

Fig. 2 Overview of the testing phase of the SRCNN scheme

B_1 is an n_1-dimensional vector. The rectified linear unit (ReLU, $(\max(0, x))$ [22] was used as an activation function.

In the non-linear mapping step, the n_1-dimensional feature vectors are mapped non-linearly to another set of n_2-dimensional feature vectors, called the high-resolution features. The operation of the second step is as follows:

$$F_2(Y) = \max(0, W_2 * F_1(Y) + B_2). \quad (2)$$

Here W_2, which has a size of $n_1 \times f_2 \times f_2$, corresponds to n_2 filters, and B_2 is an n_2-dimensional vector.

The last reconstruction part aggregates these high-resolution features to generate the final high-resolution image. The operation of the last layer is as follows:

$$F(Y) = W_3 * F_2(Y) + B_3. \quad (3)$$

Here W_3, which has a size of $n_2 \times f_3 \times f_3$, corresponds to c filters, and B_3 is a c-dimensional vector.

Training Phase

Our experiments using the SRCNN scheme can be divided into a training phase and a testing phase. In the training phase, the mapping function F requires the estimation of network parameters $\Theta = \{W_1, W_2, W_3, B_1, B_2, B_3\}$. Let us define the reconstructed images $F(\mathbf{Y}; \Theta)$ and the ground-truth high-resolution image $\mathbf{X}$. The loss function L, which was the mean squared error used in this study, is given as follows:

$$L(\Theta) = \frac{1}{n} \sum_{i=1}^{n} \| F(Y_i; \Theta) - X_i \|^2, \quad (4)$$

where n is the number of training images, $\boldsymbol{X}_i$ is a set of high-resolution images, and $\boldsymbol{Y}_i$ is the set of their corresponding low-resolution images. The loss function was minimized using stochastic gradient descent with the standard backpropagation.

To explore an appropriate training scheme for improving the image quality of high-resolution images, two different training datasets, i.e., 91 non-medical images and 45 chest CT images, were used. Dong et al. proposed that the typical and basic SRCNN configuration is $f_1 = 9$, $f_2 = 1$, $f_3 = 5$, $n_1 = 64$, and $n_2 = 32$ [16]. Therefore, this SRCNN configuration was used in this study. In the training phase, the SRCNN scheme was trained using each training dataset. Finally, two types of trained SRCNN models, which were trained using non-medical image dataset and chest CT image dataset, were obtained.

Testing Phase

Figure 2 shows an overview of the testing phase. Moreover, the usefulness of the super-resolution technique has already been demonstrated in computer vision. However,

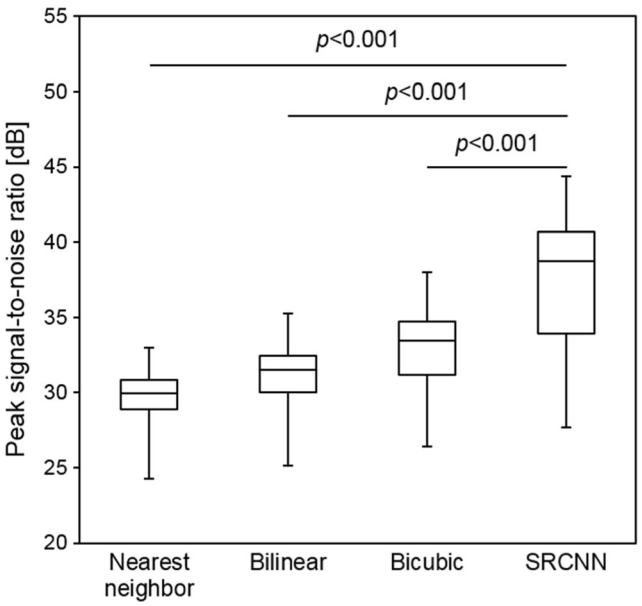

Fig. 3 Comparison of the PSNR between the linear interpolation methods and the SRCNN scheme (the SRCNN trained using the CT images), for a magnification of ×2. The SRCNN scheme yielded significantly higher PSNR than the linear interpolation methods ($p < 0.001$)

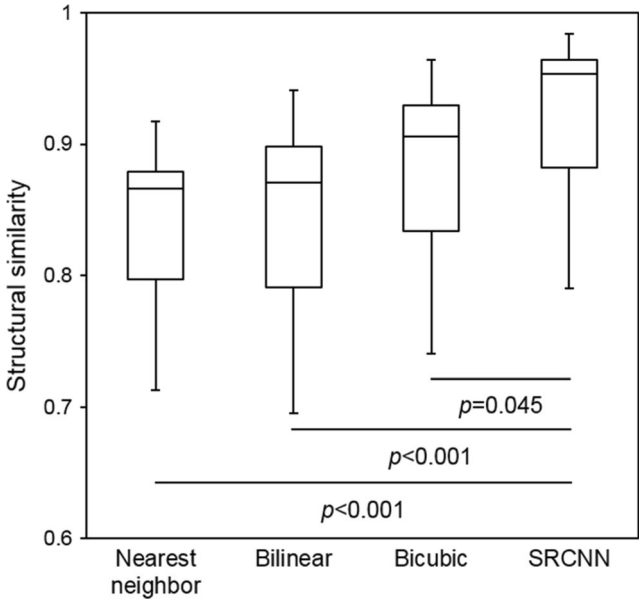

Fig. 4 Comparison of the SSIM between the linear interpolation methods and the SRCNN scheme (the SRCNN trained using the CT images), for a magnification of ×2. The SRCNN scheme yielded significantly higher SSIM than the linear interpolation methods ($p < 0.001$, or $p < 0.05$)

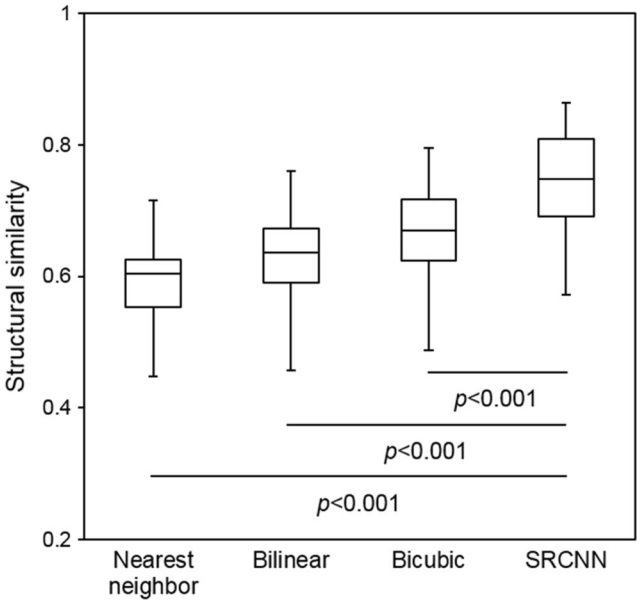

Fig. 6 Comparison of the SSIM between the linear interpolation methods and the SRCNN scheme (the SRCNN trained using the CT images), for a magnification of ×4. The SRCNN scheme yielded significantly higher SSIM than the linear interpolation methods ($p < 0.001$)

for the application of the super-resolution technique to medical images, the evaluation of the super-resolution technique in medical images poses a difficult problem owing to the uncertainty in terms of accuracy of the resulting high-resolution image obtained with the super-resolution scheme. Therefore, the following image-restoration experiment was performed using the down-sampled original test image.

In the testing phase, 44 chest CT images (matrix size: 512 × 512 pixels) were used. First, two types of low-resolution images were generated by down-sampling performed using the bicubic interpolation method. The matrix

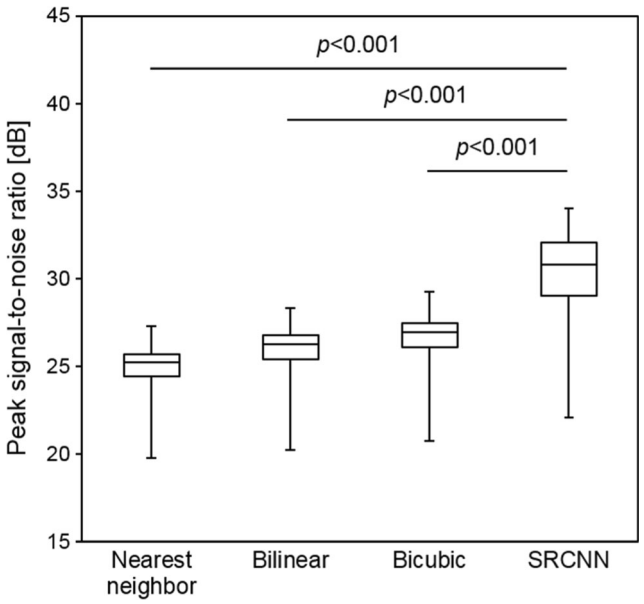

Fig. 5 Comparison of the PSNR between the linear interpolation methods and the SRCNN scheme (the SRCNN trained using the CT images), for a magnification of ×4. The SRCNN scheme yielded significantly higher PSNR than the linear interpolation methods ($p < 0.001$)

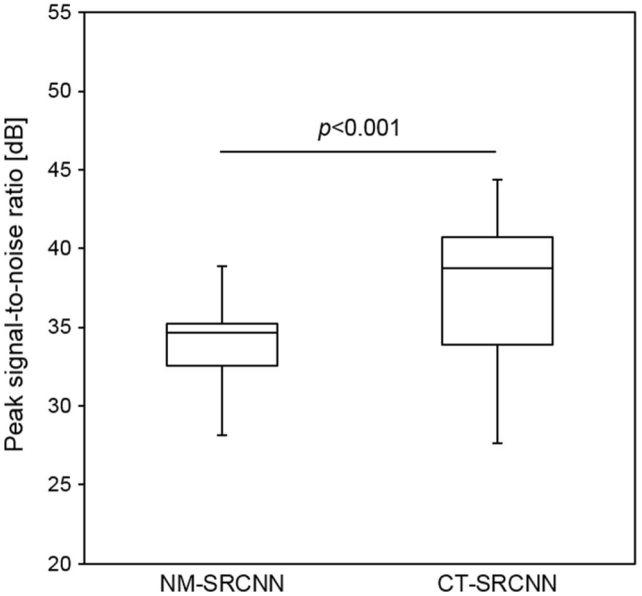

Fig. 7 Comparison of the PSNR between the training of the SRCNN using non-medical images (NM-SRCNN) and the training of the SRCNN using CT images (CT-SRCNN), for a magnification of ×2. The CT-SRCNN yielded significantly higher PSNR than the NM-SRCNN ($p < 0.001$)

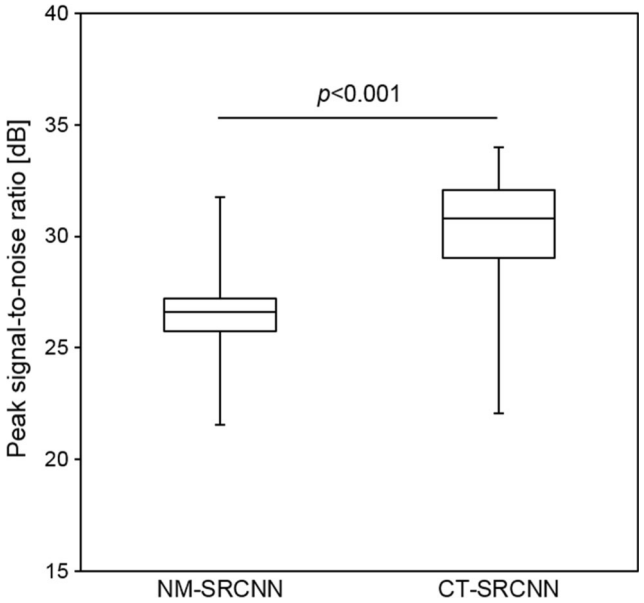

Fig. 8 Comparison of the PSNR between the training of the SRCNN using non-medical images (NM-SRCNN) and the training of the SRCNN using CT images (CT-SRCNN), for a magnification of ×4. The CT-SRCNN yielded significantly higher PSNR than the NM-SRCNN ($p < 0.001$)

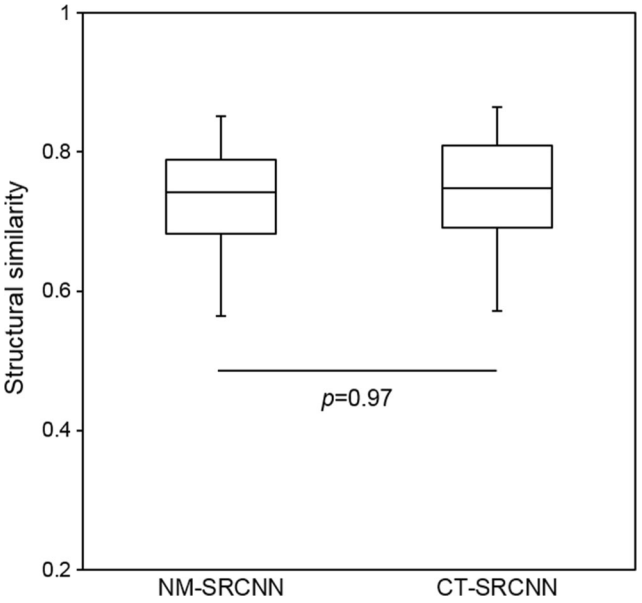

Fig. 10 Comparison of the SSIM between the training of the SRCNN using non-medical images (NM-SRCNN) and the training of the SRCNN using CT images (CT-SRCNN), for a magnification of ×4. The CT-SRCNN yielded marginally higher SSIM than the NM-SRCNN. However, the difference between the NM-SRCNN and the CT-SRCNN was not statistically significant ($p = 0.97$)

sizes of the resulting low-resolution image were 256 × 256 pixels and 128 × 128 pixels. Next, the high-resolution images were reconstructed from the down-sampled low-resolution image by using the trained SRCNN scheme for a ×2 magnification or for a ×4 magnification. Thus, the matrix size of the resulting high-resolution image was the same size as that of the original test image—512 × 512 pixels. Such experiments enable us to assess whether the resulting high-resolution image was correctly restored or not, in comparison with the original image. Finally, the image restoration quality of the resulting high-resolution image was quantitatively assessed by measuring the image quality metrics using the original test image as the ground-truth image.

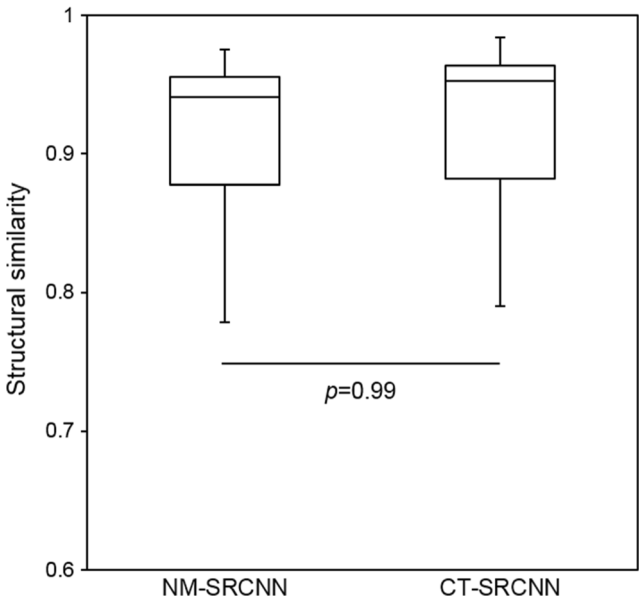

Fig. 9 Comparison of the SSIM between the training of the SRCNN using non-medical images (NM-SRCNN) and the training of the SRCNN using CT images (CT-SRCNN), for a magnification of ×2. The CT-SRCNN yielded marginally higher SSIM than the NM-SRCNN. However, the difference between the NM-SRCNN and the CT-SRCNN was not statistically significant ($p = 0.99$)

Evaluation Methods

To quantitatively evaluate the resulting high-resolution images, two image quality metrics were used, i.e., peak signal-to-noise ratio (PSNR) [23] and structural similarity (SSIM) [24]. These metrics are widely used for objectively evaluating the image quality. PSNR is most commonly used as a measure of the quality of noisy images [25]. SSIM indicates the similarity between two images for assessing the perceptual image quality.

For a comparative evaluation of the SRCNN scheme and the conventional linear interpolation methods, the same experiments were performed using the liner interpolation methods, i.e., the nearest neighbor, bilinear, and bicubic interpolations. The image quality metrics of the SRCNN scheme on the test dataset were compared with those of the conventional linear interpolation methods.

Statistical Analysis

The statistical significance of the differences in the image quality metrics between the SRCNN scheme and the linear interpolation

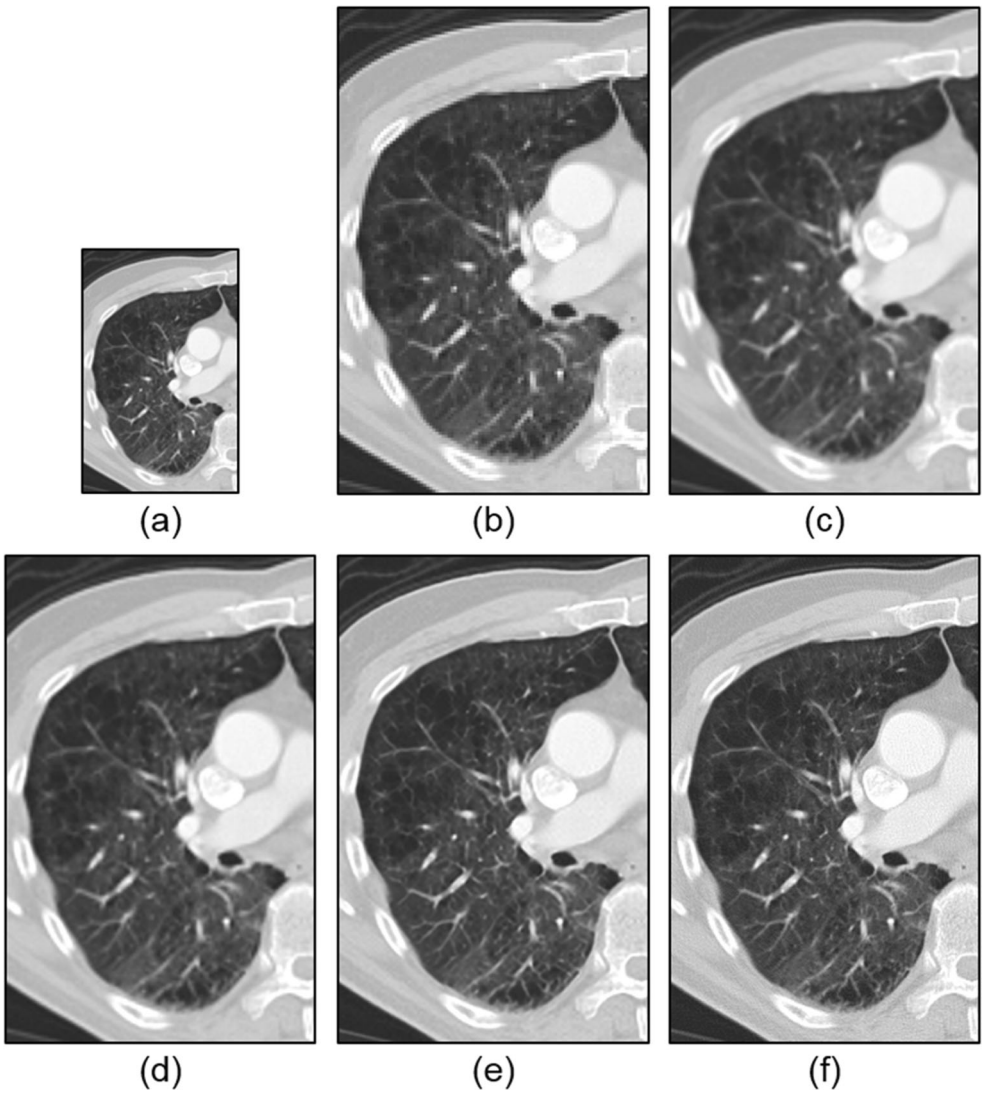

Fig. 11 An example of the reconstructed high-resolution images for a magnification of ×2. **a** Low-resolution image, **b** nearest neighbor, **c** bilinear, **d** bicubic, **e** the SRCNN scheme (CT-SRCNN), and **f** original test image (the ground-truth image)

methods was tested using one-way analysis of variance and Tukey's post hoc test. The statistical significance of the differences in the image quality between the SRCNN trained using non-medical images and the SRCNN trained using CT images was tested by Student's *t* test. All statistical analyses were conducted using IBM SPSS Statistics version 22.0 (IBM Corp., Armonk, NY). For all comparisons, $p < 0.05$ was considered to indicate a statistically significant difference. Data are presented as mean ± standard deviation (SD).

Results

Comparison of Image Quality

Figures 3 and 4 represent the PSNRs and the SSIMs of the linear interpolation methods and the SRCNN scheme (the SRCNN trained using CT images), respectively, for a ×2 magnification. As shown in these figures, the SRCNN scheme demonstrated a performance superior to that of the three linear interpolation methods. In the PSNR, the mean ± SD of the nearest neighbor, the bilinear, the bicubic, and the SRCNN scheme were 29.87 ± 1.70, 31.25 ± 2.02, 32.98 ± 2.41, and 37.42 ± 4.17 dB, respectively (Fig. 3). The differences in the PSNR between the three linear interpolation methods and the SRCNN scheme were statistically significant ($p < 0.001$). In the SRCNN scheme, the mean ± SD of the SSIM was 0.920 ± 0.059, which was significantly higher than that of the nearest neighbor (0.837 ± 0.060. $p < 0.001$), the bilinear (0.843 ± 0.073, $p < 0.001$), and the bicubic (0.878 ± 0.068, $p = 0.045$) (Fig. 4).

Figures 5 and 6 represent the PSNRs and the SSIMs of the linear interpolation methods and the SRCNN scheme (the SRCNN trained using CT images), respectively, for a ×4 magnification. As shown in these figures, the SRCNN scheme also yielded higher image quality compared to that of the three linear interpolation methods for a ×4 magnification. In the PSNR, the mean ± SD of the nearest neighbor, the bilinear,

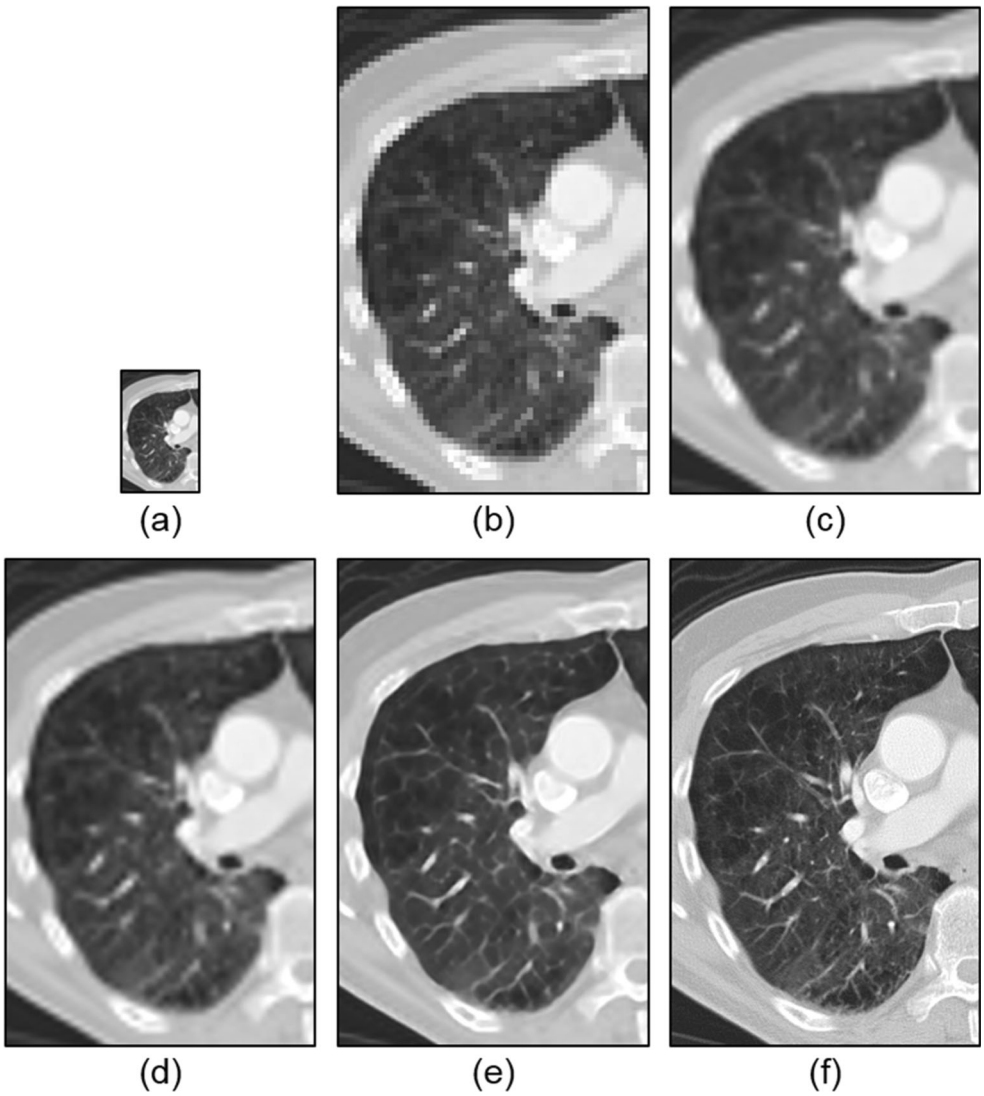

Fig. 12 An example of the reconstructed high-resolution images for a magnification of ×4. **a** Low-resolution image, **b** nearest neighbor, **c** bilinear, **d** bicubic, **e** the SRCNN scheme (CT-SRCNN), and **f** original test image (the ground-truth image)

the bicubic, and the SRCNN scheme were 25.04 ± 1.46, 26.01 ± 1.58, 26.76 ± 1.64, and 30.50 ± 2.42 dB, respectively (Fig. 5). The differences in the PSNR between the three linear interpolation methods and the SRCNN scheme were statistically significant ($p < 0.001$). In the SSIM, the mean ± SD of the nearest neighbor, the bilinear, the bicubic, and the SRCNN scheme were 0.590 ± 0.069, 0.627 ± 0.079, 0.663 ± 0.079, and 0.746 ± 0.079, respectively (Fig. 6). The differences in the SSIM between the three linear interpolation methods and the SRCNN scheme were also statistically significant ($p < 0.001$).

Comparison of Training Schemes

Figures 7 and 8 show a comparison of the PSNRs for the SRCNN scheme trained using the non-medical image dataset (NM-SRCNN) and the SRCNN scheme trained using the chest CT image dataset (CT-SRCNN), for ×2 and ×4 magnifications, respectively. The mean ± SD of the CT-SRCNN scheme was 37.42 ± 4.17 dB, which was significantly higher than that of the NM-SRCNN scheme (34.07 ± 2.23 dB, $p < 0.001$) for a ×2 magnification (Fig. 7). For a ×4 magnification, the mean ± SD of the CT-SRCNN scheme was 30.50 ± 2.42 dB, which was also significantly higher than that of the NM-SRCNN scheme (26.54 ± 1.57 dB, $p < 0.001$) (Fig. 8).

Figures 9 and 10 show a comparison of the SSIMs for the NM-SRCNN scheme and the CT-SRCNN scheme, for ×2 and ×4 magnifications, respectively. For a ×2 magnification, the mean ± SD of the CT-SRCNN scheme was 0.920 ± 0.059, which was higher than that of the NM-SRCNN scheme (0.910 ± 0.059) (Fig. 9). For a ×4 magnification, the mean ± SD of the CT-SRCNN scheme was 0.746 ± 0.079, which was also higher than that of the NM-SRCNN scheme (0.728 ± 0.076) (Fig. 10). The difference in the SSIM between the NM-SRCNN scheme and the CT-SRCNN scheme was not statistically significant, for both ×2 and ×4 magnifications (for a magnification of ×2, $p = 0.99$; for a magnification of ×4, $p = 0.97$).

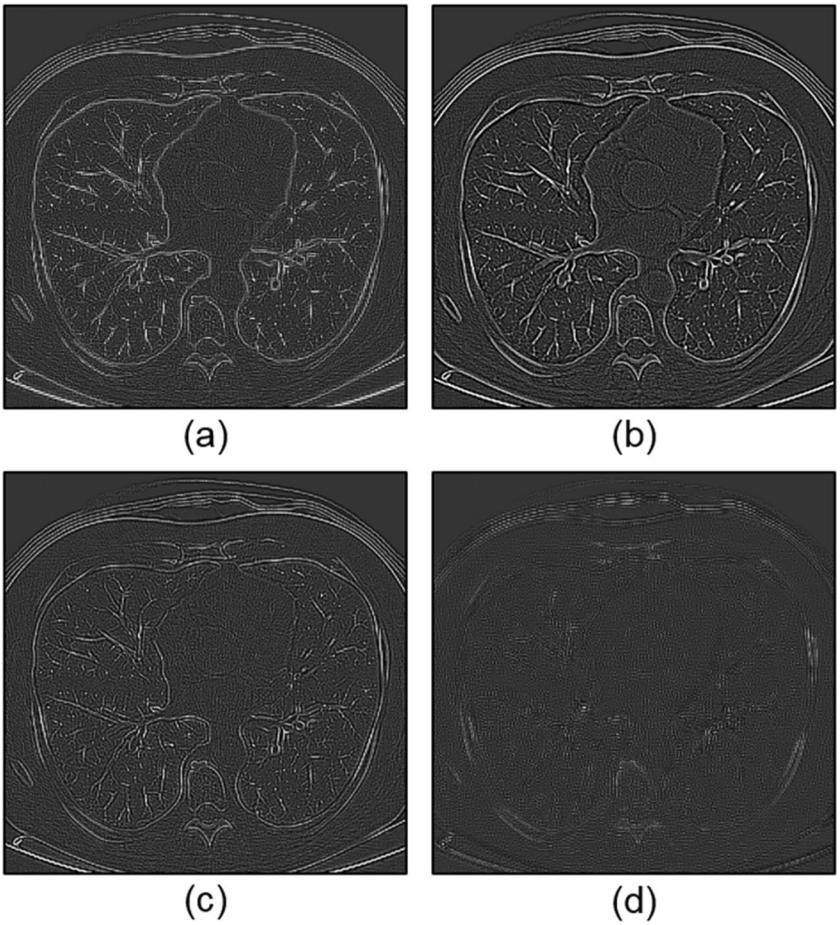

Fig. 13 An example of the subtraction images between the original test image and **a** nearest neighbor, **b** bilinear, **c** bicubic, and **d** the SRCNN scheme (CT-SRCNN), for a magnification of ×2

Visual Examples

Figures 11 and 12 illustrate an example of the resulting high-resolution images in the lung field obtained using the three linear interpolation methods and the SRCNN scheme (the SRCNN trained using CT images), for magnifications of ×2 and ×4, respectively. For a magnification of ×2, the SRCNN scheme yielded much sharper edges compared to those obtained using the linear interpolation methods. Visual assessment confirmed that the SRCNN scheme restored close to the original image at a higher level in comparison with the linear interpolation methods (Fig. 11). For a magnification of ×4, the resulting high-resolution image by the linear interpolation methods was clearly a lower quality image in comparison with the original image. In particular, the nearest neighbor generated an over-smoothed image with a jagged artifact, whereas with the application of the SRCNN scheme, the lung structures could be observed in higher detail in the resulting high-resolution image as compared to that with the linear interpolation methods (Fig. 12).

Figures 13 and 14 illustrate an example of subtraction images that are obtained from the high-resolution image by each method from the original reference image, for magnifications of ×2 and ×4, respectively. These figures visualize the components lost from the original image for each method. As shown in these figures, the conventional linear interpolation methods lost most of the high-frequency components due to up-sampling. On the other hand, the SRCNN scheme yielded high image quality without compromising the high-frequency components in the original image, for magnifications of both ×2 and ×4.

Discussion

In this study, the SRCNN scheme, which is the state-of-the-art super-resolution method in computer vision, was used for enhancing image resolution in chest CT images. The SRCNN scheme used in this study yielded significantly higher image quality over the conventional linear interpolation methods, for magnifications of both ×2 and ×4. These results indicated that the SRCNN scheme significantly outperforms the linear interpolation methods for enhancing image resolution in chest CT images. Recent studies have shown that similar results were obtained in non-medical images [16], and in chest radiographs [17, 18].

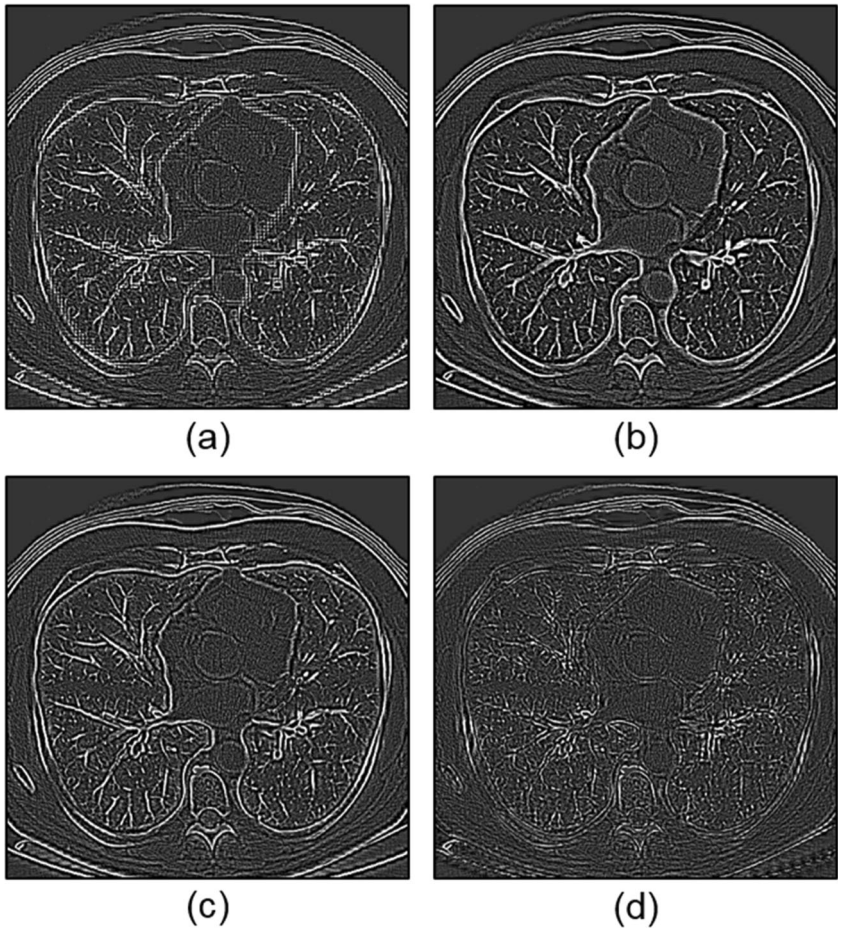

Fig. 14 An example of the subtraction images between the original test image and **a** nearest neighbor, **b** bilinear, **c** bicubic, and **d** the SRCNN scheme (CT-SRCNN), for a magnification of ×4

Two types of training schemes—using non-medical images or chest CT images—were used for training the SRCNN. In PSNR, the training of the SRCNN using CT images yielded significantly higher image quality than the training of the SRCNN using non-medical images. In SSIM, the training of the SRCNN using CT images yielded marginally higher image quality than the training of the SRCNN using non-medical images. These results suggest that the training of the SRCNN scheme using a dataset that is similar to target images provides an effective training method for improving the image quality of the reconstructed high-resolution images.

The reconstructed high-resolution image obtained with the SRCNN scheme was highly restored compared to the original reference image, in particular for a magnification of ×2. The subtraction image obtained from the high-resolution images by using each method from the original reference image showed that the SRCNN scheme yielded high-resolution images that were very close to the original reference image, without any obvious artifacts. These results demonstrate that the SRCNN scheme provides an effective and robust approach for enhancing image resolution in CT images without generating obvious artifacts. Therefore, the SRCNN scheme may provide a potential approach for yielding a high-resolution CT image from a standard CT image.

However, this study has a few limitations. A previous study on non-medical images showed that the architecture of the deeper SRCNN model did not result in high performance because it was difficult to set appropriate learning rates in the training of the deeper SRCNN model [16]. Therefore, the basic and typical SRCNN configurations were used in the proposed computer vision study. However, to use the SRCNN scheme for other CT images, further study is needed to identify the optimal network configuration for CT images.

Additionally, to use the SRCNN scheme, the input images are required to have the same 2D sizes as well as non-medical images. Therefore, in this study, the SRCNN scheme was applied to 2D CT images. For enhancing image resolution in volumetric 3D CT images, it is necessary to design a new 3D SRCNN that can learn the 3D volumetric data directly.

Furthermore, the number of training images in this study was relatively small. In general, deep learning benefits from training on a large dataset. The SRCNN scheme can also deal with a large training dataset in comparison with existing example-based super-resolution methods. Therefore, the results of this study must be validated using a larger dataset. These issues will be addressed in for future studies.

Conclusions

In this study, the SRCNN scheme was applied for enhancing image resolution in chest CT images. The experimental results obtained using clinical CT images demonstrated that the SRCNN scheme significantly outperforms conventional linear interpolation methods when used for enhancing the image resolution in chest CT images. In the experiments conducted as part of this study, the SRCNN scheme could restore very close to the reference image. The results demonstrate the potential applications of the SRCNN scheme for generating high-resolution CT images from standard CT images.

References

1. Park SC, Park MK, Kang MG: Super-resolution image reconstruction: a technical overview. IEEE Signal Process Mag 20(3):21–36, 2003
2. Yeh JJ, Chen SCC, Teng WB, Chou CH, Hsieh SP, Lee TL, Wu MT: Identifying the most infectious lesions in pulmonary tuberculosis by high-resolution multi-detector computed tomography. Eur Radiol 20(9):2135–2145, 2010
3. Akira M, Inoue Y, Arai T, Sugimoto C, Tokura S, Nakata K, Kitaichi M: Osaka respiratory diseases symposia group: pulmonary fibrosis on high-resolution CT of patients with pulmonary alveolar proteinosis. AJR 207(3):544–551, 2016
4. Lee HY, Lee KS, Jeong YJ, Hwang JH, Kim HJ, Chung MP, Han J: High-resolution CT findings in fibrotic idiopathic interstitial pneumonias with little honeycombing: serial changes and prognostic implications. AJR 199(5):982–989, 2012
5. Mathieson JR, Mayo JR, Staples CA, Müller NL: Chronic diffuse infiltrative lung disease: comparison of diagnostic accuracy of CT and chest radiography. Radiology 171(1):111–116, 1989
6. Itoh H, Murata K, Konishi J, Nishimura K, Kitaichi M, Izumi T: Diffuse lung disease: pathologic basis for the high-resolution computed tomography findings. J Thorac Imaging 8(3):176–188, 1993
7. Sverzellati N: Highlights of HRCT imaging in IPF. Respir Res 14(1):S3, 2013
8. Siu WC, Hung KW: Review of image interpolation and super-resolution. Proceedings of the 2012 Asia Pacific Signal & Information Processing Association Annual Summit and Conference: 1–10, 2012
9. Roweis ST, Saul LK: Nonlinear dimensionality reduction by locally linear embedding. Science 290(5500):2323–2326, 2000
10. Yang J, Wright J, Huang TS, Ma Y: Image super-resolution via sparse representation. IEEE Trans Image Process 19(11):2861–2873, 2010
11. Timofte R, De Smet V, Van Gool L: Anchored neighborhood regression for fast example-based super-resolution. Proceedings of the IEEE International Conference on Computer Vision: 1920–1927, 2013
12. Ota J, Umehara K, Ishimaru N, Ohno S, Okamoto K, Suzuki T, Shirai N, Ishida T: Evaluation of the sparse coding super-resolution method for improving image quality of up-sampled images in computed tomography. Proc SPIE 10133: 101331S-1-101331S-9, 2017
13. Xie J, Xu L, Chen E: Image denoising and inpainting with deep neural networks. Advances in Neural Information Processing Systems 25:341–349, 2012
14. Xu L, Ren JS, Liu C, Jia J: Deep convolutional neural network for image deconvolution. Advances in Neural Information Processing Systems 27:1790–1798, 2014
15. Dong C, Loy CC, He K, Tang X: Learning a deep convolutional network for image super-resolution. In European Conference on Computer Vision: 184–199, 2014
16. Dong C, Loy CC, He K, Tang X: Image super-resolution using deep convolutional networks. IEEE Trans Pattern Anal Mach Intell 38(2):295–307, 2016
17. Umehara K, Ota J, Ishimaru N, Ohno S, Okamoto K, Suzuki T, Shirai N, Ishida T: Super-resolution convolutional neural network for the improvement of the image quality of magnified images in chest radiographs. Proc SPIE 10133: 101331P-1–101331P-7, 2017
18. Umehara K, Ota J, Ishimaru N, Ohno S, Okamoto K, Suzuki T, Ishida T: Performance evaluation of super-resolution methods using deep-learning and sparse-coding for improving the image quality of magnified images in chest radiographs. Open J Med Imaging, 7(3): 100–111, 2017
19. Aerts H, Rios V, Emmanuel L, Ralph TH, Parmar C, Grossmann P, Carvalho S et al.: Data From NSCLC-Radiomics-Genomics. The Cancer Imaging Archive, 2015. https://doi.org/10.7937/K9/TCIA.2015.L4FRET6Z
20. Aerts HJWL, Velazquez ER, Leijenaar RT, Parmar C, Grossmann P, Cavalho S et al.: Decoding tumour phenotype by noninvasive imaging using a quantitative radiomics approach. Nat Commun, 5, 1–8, 2014
21. Clark K, Vendt B, Smith K, Freymann J, Kirby J, Koppel P, Moore S, Phillips S, Maffitt D, Pringle M, Tarbox L, Prior F: The Cancer Imaging Archive (TCIA): Maintaining and operating a public information repository. J Digit Imaging 26(6):1045–1057, 2013
22. Nair V, Hinton GE: Rectified linear units improve restricted boltzmann machines. Proceedings of the 27th international conference on machine learning: 807–814, 2010
23. Huynh-Thu Q, Ghanbari M: Scope of validity of PSNR in image/video quality assessment. Electronics Letters 44:800–801, 2008
24. Wang Z, Bovik AC, Sheikh HR, Simoncelli EP: Image quality assessment: from error visibility to structural similarity. IEEE Trans Image Process 13(4):600–612, 2004
25. Avcibas I, Sankur B, Sayood K: Statistical evaluation of image quality measures. J Electron Imaging 11:206–223, 2002